Journal of Petroleum Science and Technology 13(1): 37, 2023, Pages 16-26
DOI:10.22078/jpst.2023.5186.1892

Journal of Petroleum Science and Technology
Research Paper
https://jpst.ripi.ir/

Distribution of Oil, Water, and Ions Near the Neutral Calcite Surface in the Presence of Low and High Salinity Water: Molecular Dynamics Simulation

Saeed Abdolahi[1], Fariborz Rashidi[2] and Rohaldin Miri[3]

1. Amirkabir University of Technology - Mahshahr Campus, Bandar-e Mahshahr, Khuzestan, Iran

2. Department of Chemical Engineering, Amirkabir University of Technology, Tehran, Iran

3. School of Chemical Engineering, Iran University of Science and Technology (IUST), Tehran, Iran

Abstract

Low salinity water flooding has a significant impact on the recovery of carbonate reservoirs. In this paper, the molecular dynamics simulation was carried out to investigate the distribution of ions (Na^+, Cl^-, Ca^{2+}, Mg^{2+}, and SO_4^{2-}), water, and oil molecules near the calcite surface (the temperature of 360 K). The results show that the polar component of oil, compared to the non-polar components, tends more to the calcite surface. Additionally, the bulk of oil in brine-containing environments gradually moves away from the surface. Water molecules exhibit simultaneous movement towards the surface, forming two distinct layers near the surface and hydrating the calcite surface. Based on the water's radial distribution function, it can be observed that the hydrogen atom is closest to the surface within the second layer of water molecules. In contrast, the oxygen atom is in closest proximity to it in the first. Ions displayed concurrent movement towards the surface in conjunction with the motion of water molecules. The ion dispersion gives rise to the forming of an electrical double layer near the surface. Compared to other ions, the closeness of sodium and chlorine ions to the surface leads to creating a layer with a positive charge. The presence of an electrical layer induces the migration of polar oil molecules from the surface. The distribution of Mg^{2+} and Ca^{2+} ions indicates that Mg^{2+} has a stronger surface accumulation tendency than Ca^{2+}.

Keywords: Carbonate Reservoir, Low Salinity Water, Ions, Molecular Dynamics Microscopic Displacement in the Reservoir. LSWF.

Introduction

The important role of energy in shaping contemporary social and economic trends cannot be overstated. The increase in the population directly influences the demand for additional energy. The existing supplies of sustainable energy sources are insufficient to fulfill the demand, necessitating continued reliance on conventional energy sources. As demand for oil rises, traditional oil reservoir reserves decline, resulting in increased production from unconventional reservoirs and enhanced oil recovery (EOR) from conventional reservoirs. Various physical and chemical techniques exist that can potentially improve the oil recovery of reservoirs [1].

The practice of injecting water into oil reservoirs is commonly employed following the depletion of primary pressure to sustain reservoir pressure and facilitate the movement of oil toward production wells. The method above is commonly referred to as water flooding (WF), and its efficacy can be enhanced by manipulating the salinity and ionic composition of the injected water within the reservoir. Oil recovery can be improved significantly by using this method, known as Low Salinity Water Flooding (LSWF), which enhances oil-brine-rock interactions and increases attention over the past two decades [2,3]. According to the literature, LSWF salinity values range from 10000 to 57000 ppm [4,5].

Several spontaneous imbibition and core flooding tests have shown that LSWF can potentially improve oil recovery in carbonated reservoirs (CR) [6]. Several studies have identified the presence of an ideal ion for achieving successful LSWF, but only under specific circumstances [7]. Numerous studies have substantiated the existence of various mechanisms contributing to the LSWF in CR. These mechanisms include the wettability alteration of the surface rock (fluid-surface interaction) [8], interfacial tension (IFT) reduction (fluid-fluid interaction) [9], and fluid coalescence time [10]. During the WF process, some oil is trapped in the rock pores as small droplets. These droplets are named ganglia [11].

*Corresponding author: Fariborz Rashidi, Department of Chemical Engineering, Amirkabir University of Technology, Tehran, Iran

E-mail addresses: rashidi@aut.ac.ir

Received 2023-07-19, Received in revised form 2023-08-19, Accepted 2023-08-23, Available online .....

On the microscopic scale, the efficiency of LSWF depends on the accumulation and mobilization of ganglia and the formation of larger droplets. Ayirala et al. proposed a mechanism for improving oil sweep efficiency in porous media during LSWF, referred to as fluid coalescence time. In this mechanism, the effect of ions on the interface of the fluid-rock surface, wettability, fluid-fluid oil-oil, and its effect on oil mobility has been investigated. They proposed that in the LSWF, in the pore, the oil droplet is released from the rock due to the fluid-surface interaction, and then they coalesced because of the fluid-fluid interfacial interaction. Since oil mobility is related to coalescence time, the lower coalescence time of oil droplets for the individual ion, achieve the faster oil mobility. Overall, the major mechanism of effectiveness of LSWF on carbonate rocks is the wettability alteration of the surface rock from oil-wet to more water-wet [4,12]. The wettability of a rock determines how oil and water are spread across its surface and within its pores. The ultimate amount of oil that can be obtained is greatly impacted by this factor. It has been demonstrated that carboxylic acids in crude oil possess surface-active properties, enabling them to stick strongly to carbonate surfaces and induce oil-wetting [13]. Besides, previous studies have reported asphaltene adsorption from the oil on the surface rock [14]. CR's wettability is influenced by various variables, including carboxylic compounds, Acid Number (AN), and Base Number (BN) [15,16]. The wettability modification in LSWF is regulated at the molecular level by separating oil from the carbonate surface [17].

There have been a variety of mechanisms proposed to clarify the wettability alteration in CR during LSWF, such as rock dissolution [18], double layer expansion (DLE) [19], and multivalent ion exchange (MIE) [20,21]. Calcite dissolution alters wettability, increasing incremental oil recovery [22]. Although Mahani et al. [5] and Ouden et al. [23] have stated that this is not the primary mechanism in LSWF. It is recognized that a decrease in the salinity and ionic strength of injection water leads to an increase in the thickness of the double layer (Debye length) [24] and changes rocks' wettability toward water-wet [25]. According to the DLVO (Derjaguin-Landau-Verwey-Overbeek) theory [26], the electrical double layer (EDL) thickness is determined by the molecular and interionic interactions between the rock, oil, and brine. A positive disjoining pressure is caused by a decrease in the salt content of the water, resulting in a negative surface charge at the rock/brine contact.

Ion exchange at the rock/brine/oil interface causes carboxylate to be desorbed from the rock surface [27]. The potential determining ions (PDIs), Ca^{2+}, Mg^{2+}, and SO_4^{2-} [2,28], play a crucial role in changing the wettability of the rock surface when temperature rises [29]. Several studies have shown that Mg^{2+} and SO_4^{2-} are more reactive than Ca^{2+} [30], and it has been noted that the Mg^{2+} ion is more active at high temperatures than Ca^{2+} [31]. It has been suggested that in seawater, because of less electrostatic repulsion, the Ca^{2+} ion localizes close to the chalk surface, then reacts with carboxylic groups and releases organic molecules from the rock surface. The sulfate ions adsorb onto the positive sites of the calcite surface [2]. Fathi et al. [17] did not recognize the monovalent ions (Na+ and Cl-) as PDI and suggested that they may influence the effectiveness of divalent ions (Ca^{2+}, Mg^{2+}, and SO_4^{2-}). According to Karoussi and Hamouda, SO_4^{2-} positively affects LSWF in the presence of Ca^{2+} and Mg^{2+} [32]. However, SO_4^{2-} alone does not exhibit any discernible effects [32].

Zeta potential experiments by Derkani et al. [33] indicated that Ca^{2+} and Mg^{2+} act as PDI for calcite, and SO_4^{2-} can be an effective PDI for calcite surface. Several attempts have been made to find the primary mechanism behind the LSWF in CR. Because of the complicated interactions between oil, brine, and surface rocks, the primary mechanism of LSWF remains unknown [19]. To optimize LSWF, it is required to possess a comprehensive understanding of the effects of individual ions on both wettability and the detachment of oil from the rock surface.

Molecular Dynamics (MD) simulations provide valuable insight into PDI's role in CR wettability alteration. In the recent decade, MD simulation has been extensively used to investigate EOR in sandstone reservoirs and CR [34–38]. Atomistic MD simulations indicate an optimal salinity (~0.2M) in which oil/brine IFT is minimum and the contact angle of n-decane/water slab is maximum, which is helpful for LSWF [39]. To determine the impact of surface charge on the wettability change of calcite surface in the presence of various Na/Cl concentrations and n-decane as an oil phase, Zhao et al. performed equilibrium MD (EMD) and non-equilibrium MD (NEMD) simulations [40]. They emphasized the existence of an optimum salinity at which oil molecules become detached from the surface. Aminian and ZareNezhad [41] implemented the MD simulation to show the significant positive impact of AOT ionic surfactant, TiO_2 nanoparticles, and salts on IFT, oil contact, and oil detachment from the calcite surface. Koleini et al. [42] showed the effect of high salinity water (formation water) for linking oil to the calcite surface and the ability of low salinity water to break it down. Kim et al. [43] used density functional theory (DFT) and MD simulations to explain the effect of phenol and 1-naphthol on the wettability of the calcite surface.

According to their studies, phenol can act as a separation agent for oil phases within liquid mixtures and a binding agent between oil phases and calcite surfaces in mixtures of oil and water. According to MD simulations by Santos et al. [44] on the formation of EDL near the calcite walls at mesopore (4nm), the thickness of the water layer close to the walls decreases as water salinity is decreased. Li et al. [45] used the combination of MD and first-principal simulation to show the functionality of calcite-water interaction energy to the ions in LSWF. The results suggested that monovalent ions have the potential to diffuse through the water and interact with the surface due to the presence of more stable divalent ion hydrates in the water.

Additionally, they showed that the Na+ ion is responsible for the change in the wettability of calcite in the presence of brine, which contradicts the laboratory results [17]. Based on their observations, Badizad et al. [46] determined that the presence of sodium ions within the water layers adjacent to the calcite surface results in a positive surface charge of the calcite. Consequently, this positive charge facilitates the enhanced desorption of benzoic acid on the surface. Tohidi et al. [47] studied the effects of PDI ions and silica nanoparticles

on the formation of water channels through an oil layer. It was observed that PDI ions could not create a water channel through the adsorbed oil layer toward the calcite surface. In contrast, nanoparticles have been found to enhance the process of oil separation from the calcite surface, facilitate the formation of water channels, and enhance the disjoining pressure near the surface.

The intermolecular interactions of crude oil molecules are usually ignored in MD studies of wettability alteration in favor of the interactions between calcite, organic, and water molecules. Furthermore, previous research endeavors have often focused on a single element of crude oil, ignoring to account for the characteristics of crude oil as a natural substance. Ghasemi et al. [48] have identified several challenges encountered in previous MD simulations of LSWF. These challenges include the utilization of complicated rock models, the use of a mixture of oil components, the accurate representation of thermodynamic conditions in simulations, the consideration of pressure and external forces, the appropriate selection of force fields, the impacts of gases (such as CO_2 and CH_4) in simulations, and the upscaling of simulation results to larger scales. Investigating mechanisms and processes involved in wettability alteration is a matter of great importance and challenge in LSWF. Developing a predictive model is essential to achieve optimal performance in any EOR process. A comprehensive understanding of LSW necessitates the ability to predict the behavior of particles near the surface. Due to the complexity of the processes occurring at the nano-scale, pore-scale, and field scale, accurate prediction is exceedingly difficult. As a result, it becomes essential to explore various cases to gain insights into these processes.

In this study, we performed MD simulation to enhance comprehension of the interactions between ions and the calcite surface under conditions involving low salinity water (LSW), high salinity water (HSW), and oil molecules. The oil model was developed using the SARA test results to closely resemble the composition of the oil present in the reservoir. Oil molecules consist of saturates, resins, and aromatic components, and calcite is used to simulate a neutral surface. The main goal of this study is to examine how the ions are spread near the surface.

Materials and Methods

In this work, the $\{10\bar{1}4\}$ cleavage plane of calcite is utilized to model the calcite surface [49]. Calcite has various cleavage planes; compared to the other planes, the $\{10\bar{1}4\}$ plane has a neutral charge and a more significant ion density, leading to low surface energy and higher stability [50]. The calcite slab is six layers thick (16.734 Å) and measures 41.18 x 39.97 $Å^2$ in the xy plane. In order to examine the distribution of LSW, HSW, and oil molecules near the calcite surface, the HSW slab (5 Å) was initially positioned above the calcite surface along the z-axis. Then, for the referred system, oil film and LSW slab with the thickness of 10 and 20 Å, respectively, were added to the system and placed on top of the HSW-calcite system. The atomic structure of the MD system is illustrated in Figure 1.

We selected the type and number of ions based on the values reported in Zhang and Sarma's paper [52]. To get the desired salinity of LSW (43619 ppm) and HSW (201022 ppm), 1101 (with 14 Na^+, 16 Cl^-, 2 Mg^{2+} and 1 SO_4^{2-}) and 276 water molecules (with 18 Na^+, 26 Cl^- and 4 Ca^{2+}) were packed randomly in LSW and HSW slab by PACKMOL package [53]. The output of PACKMOL is the Cartesian coordinates of molecules' atoms (xyz). SARA test results were used to adjust the oil's composition (Table 1). A mixture of saturated resins and aromatic compounds is found in the results of the SARA test (Saturates-Asphaltenes-Resins-Aromatics). The oil layer consists of decane (38 molecules), toluene (29 molecules), and benzoic acid (BA, 14 molecules). Decane and toluene represent the non-polar compon In MD simulations, Newton's equations of motion are integrated to get a dynamical trajectory for a system containing N particles, and the motion of atoms is determined by the forces acting on them. ents of the oil. The wettability of calcite surfaces can be altered to be oil-wet by polar components of oil, such as carboxylic acid, as was discussed above. The change in CR's wettability was attributed to the presence of BA, which exhibited a significant interaction with the calcite surface [54]. In this study, we chose BA as the polar component of the oil model.

$$f_i = m_i \frac{d^2 r_i}{dt^2} = -\frac{\partial U(r_1, r_2, ..., r_N)}{\partial r_i} \quad (1)$$

where U is the potential energy and r is the particle's position. The forces are determined by numerical differentiation of the force fields. Force fields are mathematical expressions that describe the relationship between atom coordinates and the system's energy.

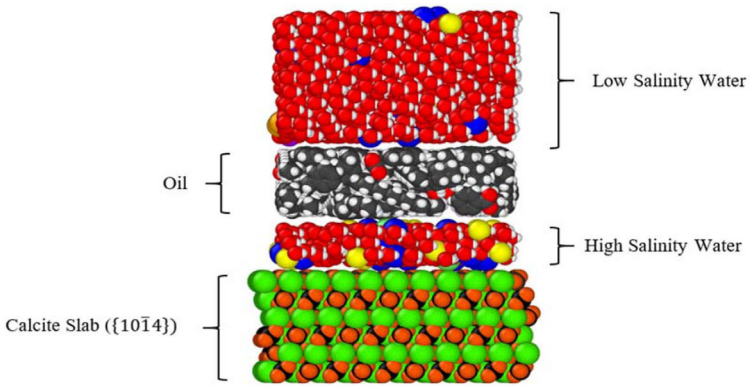

Fig. 1 Snapshot of the system simulated by MD. In this system, HSW, LSW, and oil interact with neutral calcite slab ($\{10\bar{1}4\}$). (CaCO3 with rhombohedral and parameters of a=b=4.99 Å, c=17.061 Å, α=β=90°, γ=120° [51]).

The force field is generally divided into intramolecular (bonding interaction) and intermolecular (nonbonding interaction) terms. Intramolecular potentials include bond stretching (bond between 2 atoms), angle bending (angle between 3 atoms), dihedral angle formed by 4 atoms, and improper torsion (out-of-plane motions). Intermolecular terms comprise electrostatic interactions (Coulomb's law) and van der Walls (typically Lennard-Jones interactions).We modeled calcite as a rigid body to keep the simulation from getting too intricate. Furthermore, it is not understood that the primary reason for the change in calcite's wettability in LSW is the reaction between its surface and the fluid (such as rock dissolution) [5]. The force field developed by Xiao et al. [55] was used for calcite. Although this force field has been developed for aragonite, the investigations show that it can also be used for calcite. The three-site rigid water model (TIP3P) [56], consistent with Xiao et al.'s force field, represented interactions between water molecules. The interactions of the oil phase, Na^+, Cl^-, Ca^{2+}, and Mg^{2+} were impacted by the OPLS-AA (Optimized Potentials for Liquid Simulations-All-Atom) [57] force field. For SO_4^{2-}, the force field introduced by Williams et al. [58] was adopted. The intermolecular interaction between atoms is described below:

$$U(r_{ij})=4\varepsilon_{ij}\left[\left(\frac{\sigma_{ij}}{r_{ij}}\right)^{12}-\left(\frac{\sigma_{ij}}{r_{ij}}\right)^{6}\right]+\frac{1}{4\pi\varepsilon_0}\left(\frac{q_i q_j}{r_{ij}}\right)$$

The first expression is Lennard-Jones 12−6 (LJ) potential, and the second is columbic term. The r_{ij} is the distance between two atoms.

The following formulas represent stretching of the bond, angle bending, dihedral torsion, and improper, respectively:

$$U_b=k_b\left(r-r_0\right)^2 \quad (3)$$

$$U_\theta=k_\theta(\theta-\theta_0)^2 \quad (4)$$

$$U_{dihedral}=\frac{1}{2}k_1(1+\cos(\varphi))+\frac{1}{2}k_2(1+\cos(2\varphi))+\frac{1}{2}k_3(1+\cos(3\varphi))+\frac{1}{2}k_4(1+\cos(4\varphi))U_{improper}=\kappa(\chi-\chi_0) \quad (5)$$

As shown in Figure 2, an explanation of the atom type of oil molecules is provided. Tables S1, S2, S3, S4, S5, and 6 (Supplementary material) present the mass and charge of atoms and the force fields' parameters. The LJ parameters between the different atom types are unknown, as shown in Table 2. The LJ interaction between two atoms can be calculated using the mixing rule. In this work, the cross-term potential of different atoms was obtained by applying the Lorentz-Berthelot mixing rules [59,60] as below:

$$\varepsilon_{ij}=\sqrt{\varepsilon_i\varepsilon_j} \quad (7)$$

$$\sigma_{ij}=\sqrt{\sigma_i\sigma_j} \quad (8)$$

In this paper, all the simulations were implemented by using the LAMMPS code (Large Atomic/Molecular Massively Parallel Simulator) [61]. For propagating atom positions, LAMMPS employs the Velocity-Verlet integration scheme. This method was devised by L. Verlet [62]. The new position at $t_0+\Delta t$ is equal to:

$$r_i(t+\Delta t)=r_i(t_0)+v_i(t_0)\Delta t+\frac{1}{2}a_i(t_0)\Delta t^2 \quad (9)$$

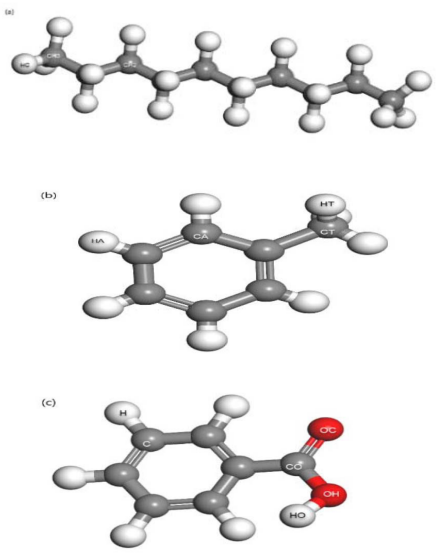

Fig. 2 Atom types of (a) Decane, (b) Toluene, (c) Benzoic acid.

Table 2 Interatomic LJ parameters for Calcite and water.

Atom Type	Atom Type	ε_{ii}	σ_{ii} [Å]
Calcite-Calcite			
$C_{calcite}$	$O_{calcite}$	6.27	1.197
$O_{calcite}$	$O_{calcite}$	0.000273	4.744
Calcite-Water			
Ca	Ow	0.269896	2.76
C	Ow	0.116079	3.46
O	Ow	0.14603	3.118
O	Hw	0.000006968	4.497

wwhere 'a' is acceleration and derived from Equation 1. The non-bonded terms of the potential energy function are the most computationally demanding part of an MD simulation. To calculate the non-bonded energy terms between each pair of atoms, the number of calculations increases as the square of the number of atoms. A preset cutoff distance is used only to consider interactions between atoms separated by less than that distance. It allows the computation to proceed more quickly. For LJ potential, a cutoff of 10 Å and the particle-particle-particle-mesh (PPPM) approach was used to calculate the long-range electrostatic interactions with a relative tolerance of 10-6 [63]. It is challenging to evaluate electrostatic interactions computationally efficiently due to Coulomb's law's long-range nature. Calculating electrostatic interactions in periodic molecular systems is done using the PPPM. The PPPM method separates interaction between charges into the sum of short-range interactions, which are computed directly by summing nearest particles and long-range interactions. An infinite system can be approximated by using a small part of the system due to periodic boundary conditions. Since water slab, oil film and rock are investigated in this study, the periodic boundary conditions were used in the x and x directions. The simulation box's Z-axis boundary constraints were fixed. Since the PPPM method can be used in periodic boundary conditions, Yeh and Berkowitz's methodology [64] was used to use the PPPM solver in the

z-direction. This method treated the system as if it had periodic atoms in z, introduced empty volumes between slabs of atoms, and removed the dipole inter-slab interactions to prevent the slab-slab interactions effectively. We built a repelling wall on the positive z-axis to keep molecules from crossing the boundary. The geometry optimization was conducted via the steepest descent approach. Then, the simulation was conducted at 360 ℃ and was performed under the canonical ensemble (NVT, fixed number of atoms, constant volume, and temperature). A system of N particles has an energy fluctuation at a constant temperature, so we must introduce this fluctuation via some mechanism. It is done by adding additional coordinates and velocities, called the Nose-Hoover thermostat [65]. The time step was 0.5 fs, which took 60 ns for the simulation to complete. Data is collected and averaged over the last 2 ns after the first 5 ns are used to equilibrate.

Results and Discussion

Utilizing a density distribution diagram is a helpful way of determining whether oil molecules have the affinity to approach the surface. Figure 3 illustrates how the number density of oil molecules varies with distance from the calcite surface along the z-axis. Based on the provided plots, it can be observed that the density peaks for the molecules decane, toluene, and BA are located at 34.25, 32.05, and 28.55 Å, respectively.

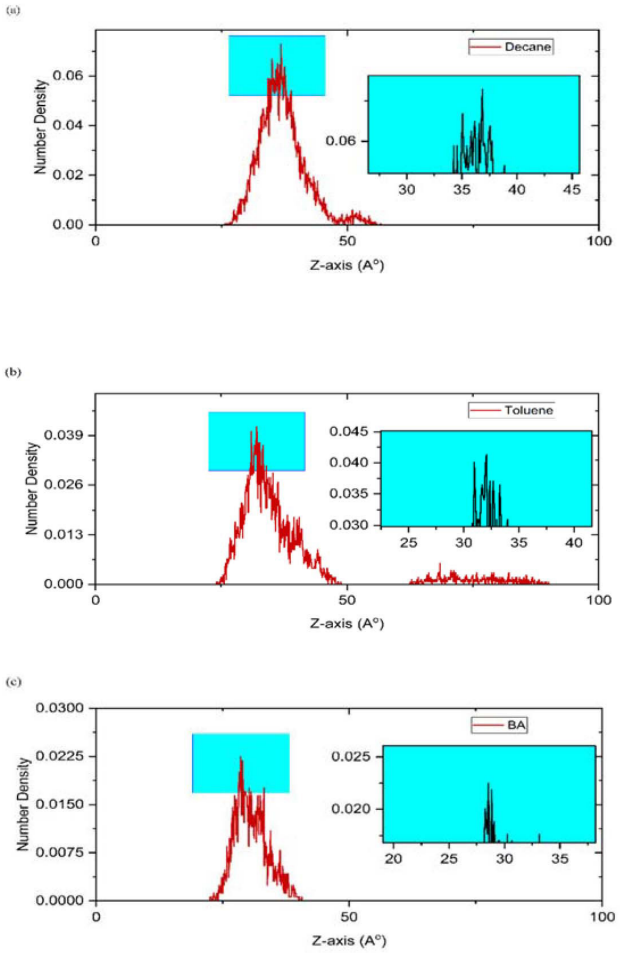

Fig. 3 Number density profile of oil molecules species adjacent to the calcite surface at (a) Decane, (b) Toluene, and (c) BA.

Through a comparative analysis of these figures, we can conclude that benzoic acid exhibits a higher affinity, compared to other oil molecules, for approaching the surface. DFT studies conducted by Ataman et al. emphasize that polar molecules such as BA have a greater affinity to approach the surface of calcite than non-polar molecules [66].

Examining the gradual change of water molecule density within the simulation box is crucial in understanding water's affinity to accumulate on surfaces. The changes in density indicate a tendency for water to move closer to the surface (Figure 4).

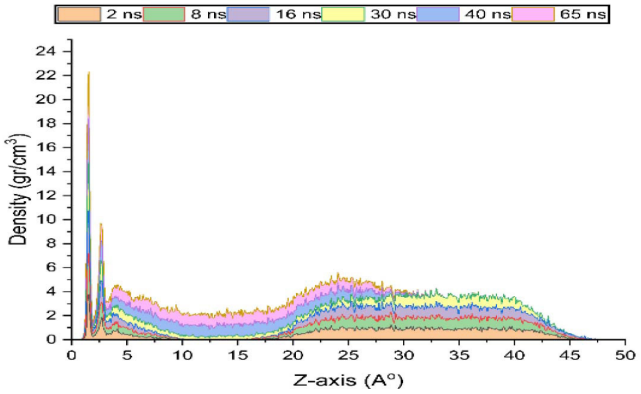

Fig. 4 Density profile of water adjacent to the calcite surface with time.

The density profile of water near the calcite surface shows a perturbation structure of water. As a result, the two major layers of water adsorbed on the surface due to the layered behavior of the water. The behavior of the water near the calcite surface has been well demonstrated using X-ray reflectivity measurements, the Crystal Truncation Rod (CTR) technique, and Atomic Force Microscopy (AFM). It confirms the MD simulation study [67–72]. The layered behavior of water is analogous to the hydration of the calcite surface and confirms the results reported by Leeuw and Parker [73]. The existence of interactions between water molecules and the surface gives rise to the formation of a transition zone. In this distance, the observation of surface effecting on fluid molecules is evident, which aligns with the findings reported by Ahmadi et al. [74]. The graph illustrates that the two primary layers of water molecules (1.55 and 2.75 Å) remain constant over time. As time passes, the height of the peaks progressively rises, and additional water molecules join the layers.

The presence of hydrogen and oxygen atoms within water molecules enhances their tendency to be involved in forming electrostatic and hydrogen bonds with calcium atoms and carbonate molecules. The Radial Distribution Function (RDF) is shown in Figure 5 to learn more about the structural characteristics of water layers. The RDF is utilized to calculate the probability that one atom is at a specific distance from the reference atom.

The RDF, g_{ij} (r), is calculated using Equation 10 [75].

$$x_i x_j \rho_N g_{ij}(r) = \frac{1}{N}\left(\sum_{k\in i}\sum_{l\in j}\delta(r_{kl}-r)\right) \quad (10)$$

The total number of atoms, the type of atom, and the number of atoms are given by the symbols N, N_i, and N_j. The mole fraction of the atom types is given by x and the atom density by N.

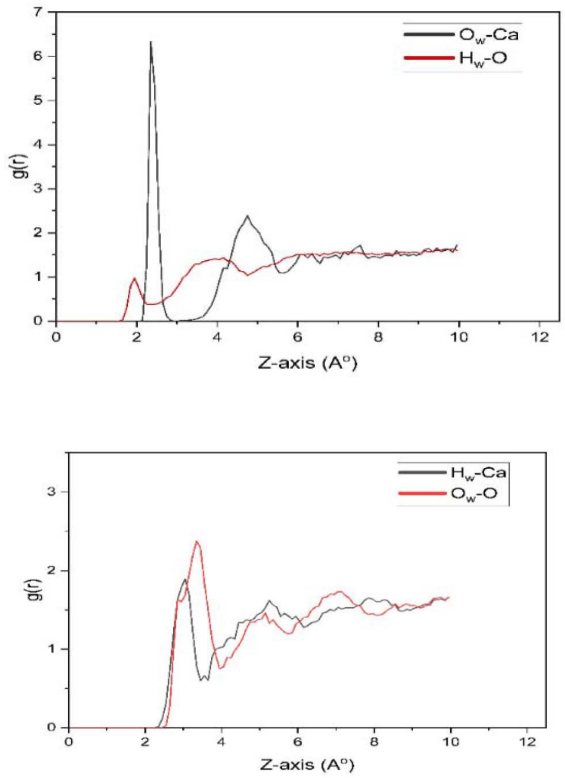

Fig. 5 (a) Plots of g(r) for atom pairs of O_w-Ca, Hw-$O_{carbonate}$, (b) Hw-Ca and O_w-$O_{carbonate}$.

A pair's distance and delta function are defined by rkl and δ, respectively. By comparing the peaks of the graphs, H_w-$O_{carbonate}$ and Ow-Ca, we can conclude that the sharp peak of hydrogen occurs at 1.95 Å of surface oxygen and 2.35 Å for oxygen from calcium. Figure 5(b) depicts the RDF plot of O_w-$O_{carbonate}$ and Hw-Ca. The sharp peak of hydrogen in water occurs at 3.05 Å of surface calcium and 3.35 Å for oxygen of water from the oxygen of carbonate. It is imperative to consider the arrangement of calcite atoms within the initial layer of the calcite slab to analyze the water molecules' orientation in the two primary layers. As previously indicated, calcite has a rhombohedral structure in its unit cell, as depicted in Figure 6. The calcium in the first layer of the calcite slab is at -0.779 Å, while the oxygen is at 0.0, -0.779, and -0.558 Å.

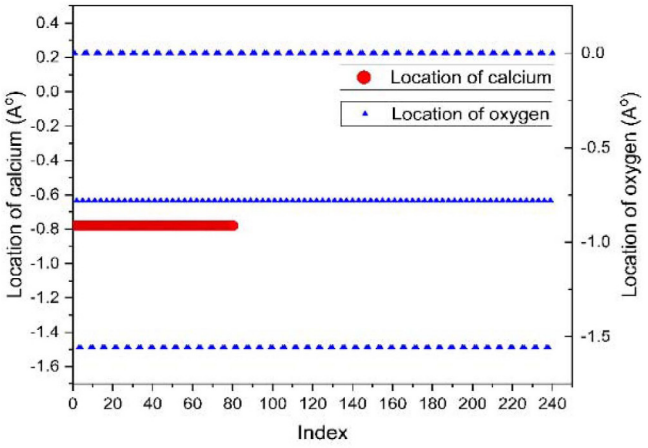

Fig. 6 Location of oxygen and calcium of the first layer of calcite.

By comparing the obtained RDF values with the location of the calcium atoms in the first layer and the nearest oxygen atoms of the carbonate ion to the surface, it is evident that the first water layer tends to move toward the surface from its oxygen side. In contrast, the second layer approaches the surface from its hydrogen side (Figure 7), consistent with Cooke et al. observations [76].

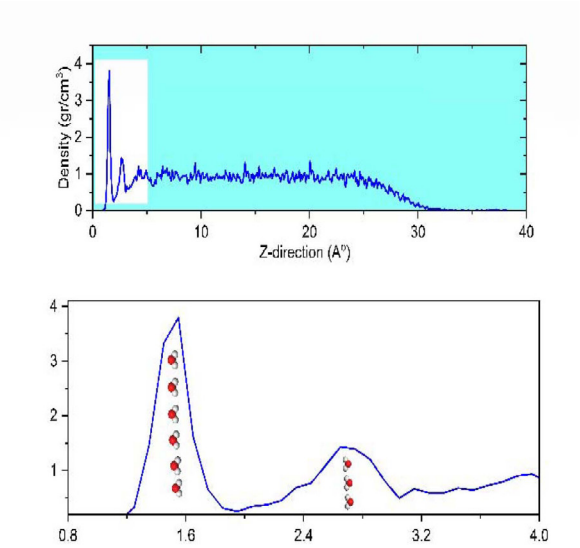

Fig. 7 Orientation of water molecules at two first layers of water adjacent to the calcite surface.

The ion dispersion of the two water layers is expected to alter when the water molecules of the low-salinity water layer enlarge and move closer to the surface. The number profile density of the ions is illustrated in Figure 8; Na^+ ions form a layer near the surface at 2.35 Å, and Cl- ions form two distinct layers at 2.05 and 4.05 Å. For Na^+, the formed layer is located between the two main layers of water. Different peaks have been created for Ca^{2+}, Mg^{2+}, and SO_4^{2-}, 3, 2, and 3. The peaks of sulfate ions are closer to the surface of calcite (3.15, 4.45, and 5.65 Å). Furthermore, it can be observed that the magnesium ion is positioned in closer proximity to the surface when compared to the calcium ion. This finding confirms the observations made by Kwak et al. [77]. They stated that the calcium ions exhibit lower reactivity with the carbonated surface than sulfate and magnesium ions at 90℃. The height and width of the sodium and chlorine ion peaks determine the electrical distribution of ions in proximity to the calcite surface. As shown in Figure 9, the presence of sodium and chlorine ions in close proximity to the surface results in the formation of a negatively charged wall close to the calcite (at 1.95 Å). The second charged wall has appeared at 2.35 Å and has a positive charge. Afterward, the negative and positive layers appeared at 4.05 and 4.55 Å, respectively. The net charge of ions in close proximity to the calcite surface is positively charged, leading to the repulsion of polar molecules, such as BA. It is caused by the higher magnitude of the second charge layer (5 e) than the first layer (3 e). Based on the observed location of the sodium and chlorine ion peaks, it can be inferred that the separation is due to the presence of sodium ions. This phenomenon is illustrated by Tohidi et al. [47] by MD simulation and Jackson et al. [78] by measuring zeta potential. The presence of these charge layers indicates the existence of the (EDL).

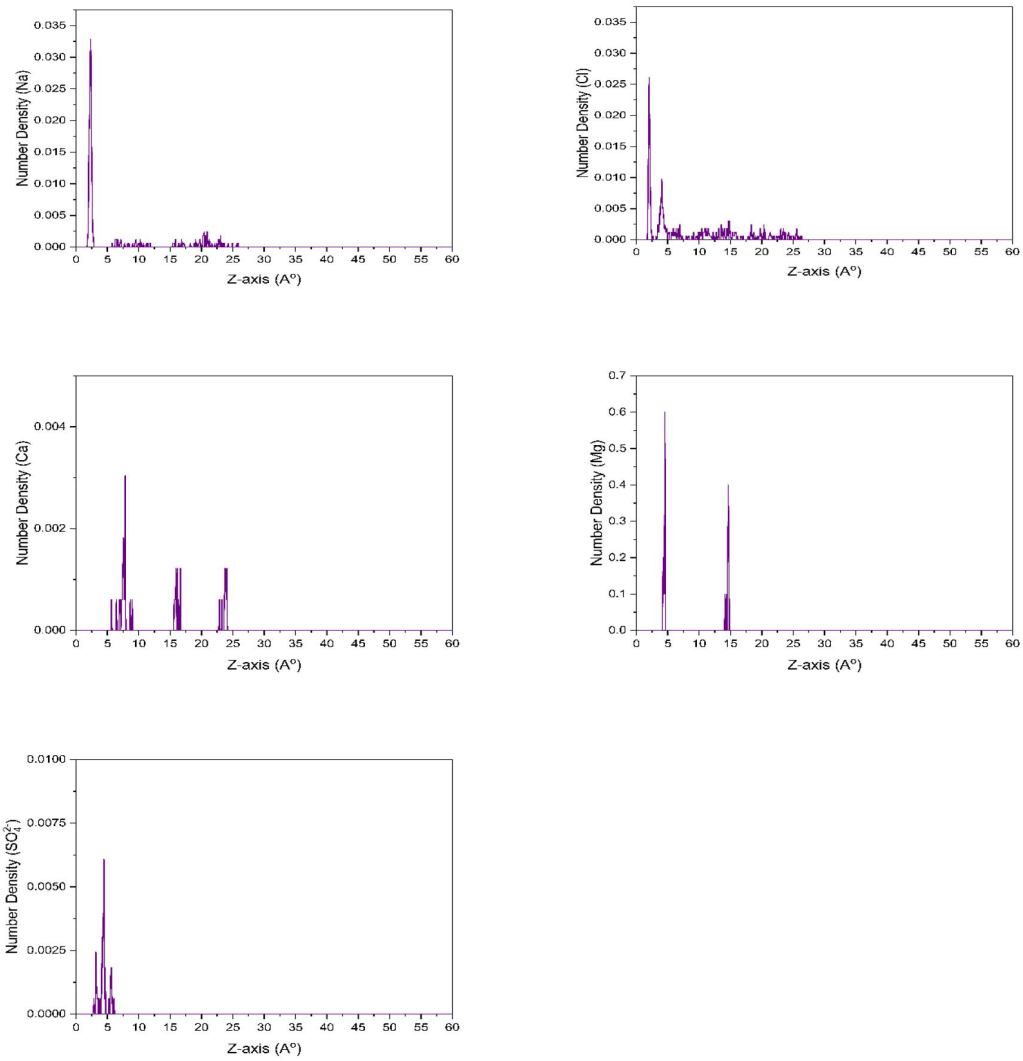

Fig. 8 Number density profile of monovalent and divalent ions (Na^+, C^{l-}, Ca^{2+}, Mg^{2+}, and SO_4^{2-}) over calcite surface.

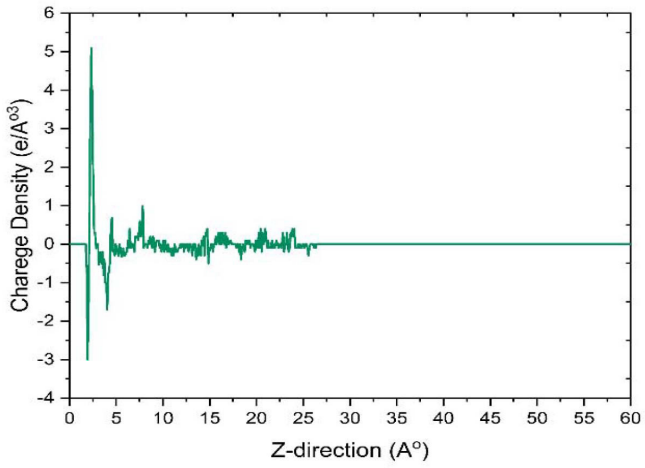

Fig. 9 Charge density distribution of monovalent and divalent ions (Na^+, C^{l-}, Ca^{2+}, Mg^{2+}, and SO_4^{2-}) over calcite surface

Conclusions

We used MD simulations to look at how the ions (Na^+, C^{l-}, Mg^{2+}, Ca^{2+}, and SO_4^{2-}), water, and oil molecules were spread out near the surface of calcite. For this purpose, high-salinity water was inserted in contact with the calcite surface. Subsequently, oil and low-salinity water were introduced to the system. We adjust the oil composition based on the SARA test results. Decane and toluene were selected as non-polar components, whereas BA was chosen as a polar component. The simulation was conducted at 360 K and was performed under the canonical ensemble (NVT). The key findings are as follows:

1) The polar component of oil exhibits a higher affinity for the surface of calcite when compared to its non-polar component.

2) Water molecules make two distinct layers near the calcite surface.

3) In the first water layer, the oxygen atom is closer to the surface, while in the second layer, the hydrogen atom assumes a closer proximity to the surface.

4) The formation of an electrical double layer near the surface results in a movement of polar oil molecules away from it.

5) The sodium and chloride ions are closer to the surface than other ions, forming an interface with the positive charge.

This study investigated the behavior and distribution of ions in the presence of oil and near-neutral calcite surfaces. However, experimental research utilizing MD simulations will be necessary to investigate a particular system comprehensively. Given that the force field designed for calcite is tailored to specific systems, it is recommended to use a quantum-mechanical atomistic simulation method to obtain a deeper knowledge of the calcite's interactions with ions, oil, and water.

Nomenclatures

U: Potential Energy [kcal/mol]
f: Force [Kcal/mole-Angstrom]
m: Mass
r: Position of particle, Atom-atom distance [Å]
t: Time [s]
q: Charge [C]
a: Acceleration [Kcal/mole^2-Angstrom]
kb: Bonded stretch parameter [kcal/(mol·Å^2)]
kθ: Angle bend parameter [kcal/(mol·deg^2)]
k1, k2, k3, k4 : Dihedral parameter [kcal/mol]
K: Improper parameter [kcal/mol]
N: Number of atoms
x: Mole fraction
g: Radial distribution function

Greek Letters

ε0: Vacuum permittivity [F Å-1]
ϵ: Minimum energy of Lennard Jones potential [kcal/mol]
σ: Lennard Jones diameter [Å]
θ: Radius [deg]
φ: Radius [deg]
χ0: Radius [deg]
ρN: Density of atoms
δ: Delta function
π: Pi number [3.14]

Subscripts and Superscripts

i,j: Type of atom
k,l: Counter
x, y, z: x-axis, y-axis, z-axis

Abbreviations

EOR: Enhanced Oil Recovery
WF: Water Flooding
LSWF: Low Salinity Water Flooding
CR: Carbonated Reservoir
IFT: Interfacial Tension
DLE: Double-layer expansion
MIE: Multivalent Ion Exchange
DLVO: Derjaguin-Landau-Verwey-Overbeek
EDL: Electrical Double Layer
PDI: Potential determining ion
MD: Molecular Dynamics
EMD: Equilibrium Molecular Dynamics
NEMD: Non-Equilibrium Molecular Dynamics
DFT: Density functional theory
LSW: Low Salinity Water
HSW: High Salinity Water
SARA: Saturates-Asphaltenes-Resins-Aromatics
BA: Benzoic Acid
LAMMPS: Large Atomic/Molecular Massively Parallel Simulator
LJ: Lennard Jones
TIP3P: Transferable Intermolecular Potential 3-Point
OPLS-AA: Optimized Potentials for Liquid Simulations-All-Atom
PPPM: Particle-Particle-Particle-Mesh
NVT: Canonical ensemble (Fix N, constant V and constant T)
CTR: Crystal Truncation Rod
AFM: Atomic Force Microscopy
RDF: Radial Distribution Function

References

1. Green, D. W., & Willhite, G. P. (1998). Enhanced oil recovery, 6, 143-154, Richardson, TX: Henry L. Doherty Memorial Fund of AIME, Society of Petroleum Engineers, ISBN: 978-1-61399-494-8.
2. Zhang, P., Tweheyo, M. T., & Austad, T. (2007). Wettability alteration and improved oil recovery by spontaneous imbibition of seawater into chalk: Impact of the potential determining ions Ca^{2+}, Mg^{2+}, and SO_4^{2-}. Colloids and Surfaces A: Physicochemical and Engineering Aspects, 301(1-3), 199-208, doi.org/10.1016/j.colsurfa.2006.12.058.
3. Sharma, H., & Mohanty, K. K. (2018). An experimental and modeling study to investigate brine-rock interactions during low salinity water flooding in carbonates. Journal of Petroleum Science and Engineering, 165, 1021-1039,. https://doi.org/https://doi.org/10.1016/j.petrol.2017.11.052.
4. Yousef, A. A., Al-Saleh, S., Al-Kaabi, A., & Al-Jawfi, M. (2010, October). Laboratory investigation of novel oil recovery method for carbonate reservoirs, In Canadian Unconventional Resources and International Petroleum Conference, OnePetro, doi.org/10.2118/137634-MS.
5. Mahani, H., Keya, A. L., Berg, S., Bartels, W. B., Nasralla, R., & Rossen, W. R. (2015). Insights into the mechanism of wettability alteration by low-salinity flooding (LSF) in carbonates. Energy & Fuels, 29(3), 1352-1367, doi.org/10.1021/ef5023847.
6. Gandomkar, A., & Rahimpour, M. R. (2015). Investigation of low-salinity waterflooding in secondary and tertiary enhanced oil recovery in limestone reservoirs, Energy & Fuels, 29(12), 7781-7792, doi.org/10.1021/acs.energyfuels.5b01236.
7. Austad, T., Shariatpanahi, S. F., Strand, S., Black, C. J. J., & Webb, K. J. (2012). Conditions for a low-salinity enhanced oil recovery (EOR) effect in carbonate oil reservoirs, Energy & Fuels, 26(1), 569-575, doi.org/10.1021/ef201435g.
8. Yousef, A. A., Al-Saleh, S., Al-Kaabi, A., & Al-Jawfi, M. (2011). Laboratory investigation of the impact of injection-water salinity and ionic content on oil recovery from carbonate reservoirs. SPE Reservoir Evaluation & Engineering, 14(05), 578-593, doi.org/10.2118/137634-PA.
9. Alotaibi, M. B., & Nasr-El-Din, H. A. (2009, June). Effect of brine salinity on reservoir fluids interfacial tension. In SPE Europec featured at EAGE Conference and Exhibition? SPE-121569 doi.org/10.2118/121569-MS.
10. Ayirala, S. C., Al-Saleh, S. H., & Al-Yousef, A. A. (2018). Microscopic scale interactions of water ions at crude oil/water interface and their impact on oil mobilization in advanced water flooding, Journal of Petroleum Science and Engineering, 163, 640-649, doi.org/https://doi.org/10.1016/j.petrol.2017.09.054.
11. Liu, F., & Wang, M. (2022). Wettability effects on mobilization of ganglia during displacement. International Journal of Mechanical Sciences, 215, 106933, doi.org/https://doi.org/10.1016/j.ijmecsci.2021.106933.
12. Al-Shalabi, E. W., & Sepehrnoori, K. (2016). A

comprehensive review of low salinity/engineered water injections and their applications in sandstone and carbonate rocks, Journal of Petroleum Science and Engineering, 139, 137-161, doi.org/https://doi.org/10.1016/j.petrol.2015.11.027.
13. Fathi, S. J., Austad, T., Strand, S., & Puntervold, T. (2010). Wettability alteration in carbonates: The effect of water-soluble carboxylic acids in crude oil. Energy & Fuels, 24(5), 2974-2979, doi.org/10.1021/ef901527h.
14. Dubey, S. T., & Waxman, M. L. (1991). Asphaltene adsorption and desorption from mineral surfaces, SPE Reservoir Engineering, 6(03), 389-395., doi.org/10.2118/18462-PA.
15. Zhang, P., & Austad, T. (2005, February). The relative effects of acid number and temperature on chalk wettability, In SPE International Conference on Oilfield Chemistry?, SPE-92999, SPE., doi.org/10.2118/92999-MS.
16. Xie, Q., He, S., & Pu, W. (2010). The effects of temperature and acid number of crude oil on the wettability of acid volcanic reservoir rock from the Hailar Oilfield, Petroleum Science, 7, 93-99, doi.org/10.1007/s12182-010-0011-2.
17. Fathi, S. J., Austad, T., & Strand, S. (2012, April). Water-based enhanced oil recovery EOR by smart water in carbonate reservoirs, In SPE EOR conference at oil and gas West Asia, OnePetro, doi.org/10.2118/154570-MS.
18. Zahid, A., Shapiro, A., & Skauge, A. (2012, April). Experimental studies of low salinity water flooding in carbonate reservoirs: A new promising approach, In SPE EOR conference at oil and gas West Asia, SPE-155625, doi.org/10.2118/155625-MS.
19. RezaeiDoust, A., Puntervold, T., Strand, S., & Austad, T. (2009). Smart water as wettability modifier in carbonate and sandstone: A discussion of similarities/differences in the chemical mechanisms, Energy & Fuels, 23(9), 4479-4485, doi.org/10.1021/ef900185q.
20. Lager, A., Webb, K. J., Black, C. J. J., Singleton, M., & Sorbie, K. S. (2008). Low salinity oil recovery-an experimental investigation1, Petrophysics-The SPWLA Journal of Formation Evaluation and Reservoir Description, 49(01), Paper Number: SPWLA-2008-v49n1a2.
21. Puntervold, T., Strand, S., Ellouz, R., & Austad, T. (2015). Modified seawater as a smart EOR fluid in chalk. Journal of Petroleum Science and Engineering, 133, 440-443, doi.org/10.1016/j.petrol.2015.06.034.
22. Puntervold, T., Strand, S., Ellouz, R., & Austad, T. (2015). Modified seawater as a smart EOR fluid in chalk, Journal of Petroleum Science and Engineering, 133, 440-443., doi.org/10.1016/j.fuel.2018.03.176.
23. Den Ouden, L., Nasralla, R. A., Guo, H., Bruining, H., & Van Kruijsdijk, C. P. J. W. (2015). Calcite dissolution behaviour during low salinity water flooding in carbonate rock, In IOR 2015-18th European Symposium on Improved Oil Recovery, cp-445, European Association of Geoscientists & Engineers, doi.org/10.3997/2214-4609.201412102.
24. Stumm, W., & Morgan, J. J. (2012). Aquatic chemistry: chemical equilibria and rates in natural waters, John Wiley & Sons.
25. Tetteh, J. T., Alimoradi, S., Brady, P. V., & Ghahfarokhi, R. B. (2020). Electrokinetics at calcite-rich limestone surface: Understanding the role of ions in modified salinity waterflooding. Journal of Molecular Liquids, 297, 111868, doi.org/https://doi.org/10.1016/j.molliq.2019.111868.
26. Derjaguin, B. V. (1941). Theory of the stability of strongly charged lyophobic sol and of the adhesion of strongly charged particles in solutions of electrolytes, Acta phys. chim. URSS, 14, 633.
27. Lager, A., Webb, K. J., & Black, C. J. J. (2007, April). Impact of brine chemistry on oil recovery, In IOR 2007-14th European symposium on improved oil recovery, 24, European Association of Geoscientists & Engineers, doi.org/10.3997/2214-4609-pdb.24.A24.
28. Strand, S., Puntervold, T., & Austad, T. (2008). Effect of temperature on enhanced oil recovery from mixed-wet chalk cores by spontaneous imbibition and forced displacement using seawater, Energy & Fuels, 22(5), 3222-3225, doi.org/10.1021/ef800244v.
29. Tweheyo, M. T., Zhang, P., & Austad, T. (2006, April). The effects of temperature and potential determining ions present in seawater on oil recovery from fractured carbonates, In SPE Improved Oil Recovery Conference?, SPE-99438, doi.org/10.2118/99438-MS.
30. Shehata, A. M., Alotaibi, M. B., & Nasr-El-Din, H. A. (2014). Waterflooding in carbonate reservoirs: Does the salinity matter?, SPE Reservoir Evaluation & Engineering, 17(03), 304-313, doi.org/10.2118/170254-PA.
31. Austad, T., Strand, S., & Puntervold, T. (2009, September). Is wettability alteration of carbonates by seawater caused by rock dissolution, In Paper SCA2009-43 presented at the International Symposium of the Society of Core Analysts held in Noordwijk, The Netherlands, 27-30.
32. Karoussi, O., & Hamouda, A. A. (2007). Imbibition of sulfate and magnesium ions into carbonate rocks at elevated temperatures and their influence on wettability alteration and oil recovery, Energy & Fuels, 21(4), 2138-2146, doi.org/10.1021/ef0605246.
33. Derkani, M. H., Fletcher, A. J., Fedorov, M., Abdallah, W., Sauerer, B., Anderson, J., & Zhang, Z. J. (2019). Mechanisms of surface charge modification of carbonates in aqueous electrolyte solutions, Colloids and Interfaces, 3(4), 62, doi.org/10.3390/colloids3040062.
34. Liu, Q., Yuan, S., Yan, H., & Zhao, X. (2012). Mechanism of oil detachment from a silica surface in aqueous surfactant solutions: molecular dynamics simulations, The Journal of Physical Chemistry B, 116(9), 2867-2875, doi.org/10.1021/jp2118482.
35. Wang, S., Li, Z., Liu, B., Zhang, X., & Yang, Q. (2015). Molecular mechanisms for surfactant-aided oil removal from a solid surface, Applied Surface Science, 359, 98-105, doi.org/10.1016/j.apsusc.2015.10.068.
36. Koleini, M. M., Badizad, M. H., Kargozarfard, Z., & Ayatollahi, S. (2019). Interactions between rock/brine and oil/brine interfaces within thin brine film wetting carbonates: a molecular dynamics simulation study,

Energy & Fuels, 33(9), 7983-7992, doi.org/10.1021/acs.energyfuels.9b00496.
37. Wang, Y. F., Li, Z. Y., Zhang, S. M., Liu, D. X., & Ding, M. C. (2021). Remaining oil distribution in models with different heterogeneities after CO_2 WAG injection: visual research by nuclear magnetic resonance technique, Journal of Central South University, 28(5), 1412-1421, doi.org/10.1007/s11771-021-4712-z.
38. Abbasi, S., Khosravi-Nikou, M. R., & Shariati, A. (2023). Selective separation of propane from the propylene-propane mixture using pure silica zeolites: A molecular dynamic simulation, Chemical Engineering and Processing-Process Intensification, 184, 109294, doi.org/https://doi.org/10.1016/j.cep.2023.109294.
39. Zhao, J., Yao, G., Ramisetti, S. B., Hammond, R. B., & Wen, D. (2018). Molecular dynamics simulation of the salinity effect on the n-decane/water/vapor interfacial equilibrium. Energy & Fuels, 32(11), 11080-11092, doi.org/10.1021/acs.energyfuels.8b00706.
40. Zhao, J., Yao, G., Ramisetti, S. B., Hammond, R. B., & Wen, D. (2019). Molecular dynamics investigation of substrate wettability alteration and oil transport in a calcite nanopore, Fuel, 239, 1149-1161, doi.org/10.1016/j.fuel.2018.11.089.
41. Aminian, A., & ZareNezhad, B. (2019). Oil-detachment from the calcium carbonate surfaces via the actions of surfactant, nanoparticle and low salinity brine: an insight from molecular dynamic simulation, Chemical Engineering Science, 202, 373-382, doi.org/https://doi.org/10.1016/j.ces.2019.03.031.
42. Koleini, M. M., Badizad, M. H., Ghatee, M. H., & Ayatollahi, S. (2019). An atomistic insight into the implications of ion-tuned water injection in wetting preferences of carbonate reservoirs, Journal of Molecular Liquids, 293, 111530, doi.org/https://doi.org/10.1016/j.molliq.2019.111530.
43. Kim, S., Marcano, M. C., & Becker, U. (2019). Mechanistic study of wettability changes on calcite by molecules containing a polar hydroxyl functional group and nonpolar benzene rings. Langmuir, 35(7), 2527-2537, doi.org/10.1021/acs.langmuir.8b03666.
44. Santos, M. S., Castier, M., & Economou, I. G. (2019). Molecular dynamics simulation of electrolyte solutions confined by calcite mesopores, Fluid Phase Equilibria, 487, 24-32, doi.org/10.1016/j.fluid.2019.01.001.
45. Li, H., Vovusha, H., Sharma, S., Singh, N., & Schwingenschlögl, U. (2020). Mechanism of wettability alteration of the calcite {101 [combining macron] 4} surface, Physical Chemistry Chemical Physics, 22(27), 15365-15372, doi.org/10.1039/D0CP01715A.
46. Badizad, M. H., Koleini, M. M., Greenwell, H. C., Ayatollahi, S., Ghazanfari, M. H., & Mohammadi, M. (2020). Ion-specific interactions at calcite–brine interfaces: a nano-scale study of the surface charge development and preferential binding of polar hydrocarbons. Physical Chemistry Chemical Physics, 22(48), 27999-28011, doi.org/10.1039/D0CP04828C.
47. Tohidi, Z., Jafari, A., & Omidkhah, M. (2021). Electrolyte nanofluid performance on the oil detachment from an oil-wetted carbonate surface: Water channel formation using molecular dynamics simulation. Journal of Petroleum Science and Engineering, 196, 108006, doi.org/https://doi.org/10.1016/j.petrol.2020.108006.
48. Ghasemi, M., Shafiei, A., & Foroozesh, J. (2022). A systematic and critical review of application of molecular dynamics simulation in low salinity water injection, Advances in Colloid and Interface Science, 300, 102594, doi.org/https://doi.org/10.1016/j.cis.2021.102594.
49. Markgraf, S. A., & Reeder, R. J. (1985). High-temperature structure refinements of calcite and magnesite. American Mineralogist, 70(5-6), 590-600.
50. de Leeuw, N. H., & Parker, S. C. (1998). Surface structure and morphology of calcium carbonate polymorphs calcite, aragonite, and vaterite: an atomistic approach, The Journal of Physical Chemistry B, 102(16), 2914-2922, doi.org/10.1021/jp973210f.
51. Graf, D. L. (1961). Crystallographic tables for the rhombohedral carbonates, American Mineralogist, Journal of Earth and Planetary Materials, 46(11-12), 1283-1316.
52. Zhang, Y., & Sarma, H. (2012, November). Improving waterflood recovery efficiency in carbonate reservoirs through salinity variations and ionic exchanges: A promising low-cost" smart-waterflood" approach, In Abu Dhabi International Petroleum Exhibition and Conference, SPE-161631, doi.org/10.2118/161631-MS.
53. Martínez, L., Andrade, R., Birgin, E. G., & Martínez, J. M. (2009). PACKMOL: A package for building initial configurations for molecular dynamics simulations, Journal of computational chemistry, 30(13), 2157-2164, doi.org/10.1002/jcc.21224.
54. Lima, F. C. D. A., da Silva Alvim, R., & Miranda, C. R. (2020). Selective dissociation of benzoic acid on carbonate surfaces: A density functional theory perspective, Applied Surface Science, 529, 147103, doi.org/10.1016/j.apsusc.2020.147103.
55. Xiao, S., Edwards, S. A., & Gräter, F. (2011). A new transferable forcefield for simulating the mechanics of $CaCO_3$ crystals, The Journal of Physical Chemistry C, 115(41), 20067-20075, doi.org/10.1021/jp202743v.
56. Price, D. J., & Brooks III, C. L. (2004). A modified TIP3P water potential for simulation with Ewald summation, The Journal of Chemical Physics, 121(20), 10096-10103, doi.org/10.1063/1.1808117.
57. Jorgensen, W. L., Maxwell, D. S., & Tirado-Rives, J. (1996). Development and testing of the OPLS all-atom force field on conformational energetics and properties of organic liquids, Journal of the American Chemical Society, 118(45), 11225-11236, doi.org/10.1021/ja9621760.
58. Williams, C. D., Burton, N. A., Travis, K. P., & Harding, J. H. (2014). The Development of a Classical Force Field to Determine the Selectivity of an Aqueous Fe3+–Eda Complex for Tco4–and So42–. Journal of Chemical Theory and Computation, 10(8), 3345-3353, doi.org/10.1021/ct500198c.
59. Lorentz, H. A. (1881). Ueber die anwendung des satzes vom virial in der kinetischen theorie der gase, Annalen der physik, 248(1), 127-136, doi.org/https://doi.org/10.1002/andp.18812480110.

60. D. Berthelot, Sur le mélange des gaz, Compt. Rendus. 126 (1898) 15.
61. Plimpton S., Fast Parallel Algorithms for Short-Range Molecular Dynamics, Journal of computational physics, 117 (1995) 1–19, doi.org/10.1006/jcph.1995.1039.
62. Swope, W. C., Andersen, H. C., Berens, P. H., & Wilson, K. R. (1982). A computer simulation method for the calculation of equilibrium constants for the formation of physical clusters of molecules: Application to small water clusters, The Journal of Chemical Physics, 76(1), 637-649, doi.org/10.1063/1.442716.
63. Hockney, R. W., & Eastwood, J. W. (2021). Computer simulation using particles. crc Press.
64. Yeh, I. C., & Berkowitz, M. L. (1999). Ewald summation for systems with slab geometry, The Journal of Chemical Physics, 111(7), 3155-3162, doi.org/10.1063/1.479595.
65. Nosé, S. (1984). A unified formulation of the constant temperature molecular dynamics methods, The Journal of chemical physics, 81(1), 511-519, doi.org/10.1063/1.447334.
66. Ataman, E., Andersson, M. P., Ceccato, M., Bovet, N., & Stipp, S. L. S. (2016). Functional group adsorption on calcite: I. Oxygen containing and nonpolar organic molecules. The Journal of Physical Chemistry C, 120(30), 16586-16596, doi.org/10.1021/acs.jpcc.6b01349.
67. Chiarello, R. P., Wogelius, R. A., & Sturchio, N. C. (1993). In-situ synchrotron X-ray reflectivity measurements at the calcite-water interface, Geochimica et Cosmochimica Acta, 57(16), 4103-4110, doi.org/10.1016/0016-7037(93)90356-2.
68. Chiarello, R. P., & Sturchio, N. C. (1995). The calcite ($10\bar{1}4$) cleavage surface in water: Early results of a crystal truncation rod study, Geochimica et Cosmochimica Acta, 59(21), 4557-4561.doi.org/10.1016/0016-7037(95)00363-5.
69. Fenter, P., Geissbühler, P., DiMasi, E., Srajer, G., Sorensen, L. B., & Sturchio, N. C. (2000). Surface speciation of calcite observed in situ by high-resolution X-ray reflectivity. Geochimica et Cosmochimica Acta, 64(7), 1221-1228, doi.org/10.1016/S0016-7037(99)00403-2.
70. Liang, Y., & Baer, D. R. (1997). Anisotropic dissolution at the CaCO3 ($10\bar{1}4$)—water interface, Surface Science, 373(2-3), 275-287, doi.org/10.1016/S0039-6028(96)01155-7.
71. Hillner, P. E., Gratz, A. J., Manne, S., & Hansma, P. K. (1992). Atomic-scale imaging of calcite growth and dissolution in real time. Geology, 20(4), 359-362, doi.org/10.1130/0091-7613(1992)020<0359:ASIOCG>2.3.CO;2.
72. Reischl, B., Raiteri, P., Gale, J. D., & Rohl, A. L. (2019). Atomistic simulation of atomic force microscopy imaging of hydration layers on calcite, dolomite, and magnesite surfaces, The Journal of Physical Chemistry C, 123(24), 14985-14992, doi.org/10.1021/acs.jpcc.9b00939.
73. de Leeuw, N., & Parker, S. (1997). Atomistic simulation of the effect of molecular adsorption of water on the surface structure and energies of calcite surfaces, Journal of the Chemical Society, Faraday Transactions, 93(3), 467-475, doi.org/10.1039/A606573B.
74. Goltapeh, S. A., Abdolahi, S., Miri, R., & Hellevang, H. (2021). Extension of PC-SAFT equation of state to include mineral surface effect in fluid properties using molecular dynamic simulation, Sustainable Energy Technologies and Assessments, 48, 101624, doi.org/10.1016/j.seta.2021.101624.
75. Hansen J. P., I. R. B. T.T. of S.L. (Fourth E. McDonald, eds., Theory of Simple Liquids, in: Academic Press, Oxford, 2013: doi.org/10.1016/B978-0-12-387032-2.00013-1.
76. Cooke, D. J., Gray, R. J., Sand, K. K., Stipp, S. L. S., & Elliott, J. A. (2010). Interaction of ethanol and water with the {1014} surface of calcite, Langmuir, 26(18), 14520-14529, doi.org/10.1021/la100670k.
77. Kwak, H. T., Yousef, A. A., & Al-Saleh, S. (2014l). New insights on the role of multivalent ions in water-carbonate rock interactions, In SPE Improved Oil Recovery Conference?, 169112, doi.org/10.2118/169112-MS.
78. Jackson, M. D., Al-Mahrouqi, D., & Vinogradov, J. (2016). Zeta potential in oil-water-carbonate systems and its impact on oil recovery during controlled salinity water-flooding, Scientific Reports, 6(1), 37363, doi.org/10.1038/srep37363.